JOURNAL OF GUIDANCE, CONTROL, AND DYNAMICS
Vol. 29, No. 3, May–June 2006

Dynamic Shape Control of a Morphing Airfoil Using Spatially Distributed Transducers

J. E. Hubbard Jr.*
University of Maryland, College Park, Maryland 20742-3285

A space/time transform parameterization is used to model the upper profile section of a morphing airfoil. The parameterization allows for the quantification of morphing spatial performance in terms of a spatial bandwidth. Airfoil morphing from one shape to another allows the system to use minimal energy during the process. A multivariable response matrix is then formulated for the distributed parameter system, and standard control synthesis tools are applied to achieve a robust dynamic shape controller. The space/time parameterization results in a spatially decoupled system with Fourier coefficients as inputs and orthogonal basis shapes as outputs. A proof-of-concept simulation, which demonstrates the efficacy of a dynamically commanded airfoil profile, is presented.

Nomenclature

A	=	airfoil rib cross-sectional area
C_p	=	output matrix
c_i	=	start of actuator aperture; Fourier coefficient
E	=	Young's modulus
$h(x-c)$	=	heavyside function
I	=	airfoil rib moment of Inertia
i, j, n	=	indices
L	=	airfoil rib length
m	=	macrofiber-composite actuator gain constant
q_i	=	actuator spatial distribution
T	=	in-plane tension
U_p	=	plant input vector
u	=	exogenous command signal
X_p	=	state vector
x	=	spatial coordinate
y	=	output vector, distributed output shape
β_i	=	output Fourier coefficient
Δ_i	=	actuator aperture width
$\delta(x-c)$	=	Dirac delta function
$\delta'(x-c)$	=	point moment function
$\Lambda(x)$	=	control spatial distribution
ν_n	=	time derivative of the Fourier coefficients
$\Psi_i(x)$	=	orthogonal shape functions
ω	=	temporal frequency

I. Introduction

UNMANNED aerial vehicles (UAVs) are receiving unprecedented support in recent years in large part because of their increasing utility as intelligence, reconnaissance, and surveillance platforms. As their missions become more complex, vehicle endurance, range, maneuverability, and expense become key drivers in their design and configuration. Morphing aircraft technology has drawn widespread interest as a promising technology that can allow the design of multifunction multirole vehicles.[1–3]

For this class of vehicles, airfoil design will have a major impact on vehicle performance. Low camber airfoils yields higher lift-to-drag ratios (L/D) at high speeds, whereas high camber yields higher L/D at low speeds. To effectively broaden their mission profile, UAVs will need to morph from one airfoil shape to another so as to seamlessly transition from soar to strike, observe to maneuver, and the like. Gano and Renaud, for example, have studied a concept known as the variform wing for increasing the range and endurance of UAVs.[4] Their study involved the concept of morphing a NACA23015 airfoil into the FX 60-126 airfoil using parameters of the Shadow UAV. They projected a 22.3% increase in range and a 22% increase in endurance from their morphing airfoil concept.

Vehicle designers will need to create the most effective actuator/structural designs to morph airfoils. These designs must be capable of morphing with respect to some nominal baseline shape and use minimal energy during the process.

The use of smart materials and structures has been recognized as an efficient means of designing vehicles that can be reconfigured in response to changing conditions. In limited cases adaptive structures incorporated into modern vehicle technology have resulted in improved maneuverability, increased redundancy/survivability, and reduced weight.[5,6]

Aircraft wing and airfoil morphing offer unique challenges with regard to increased control system design complexity, actuator/sensor transducer requirements, and morphing structural materials. Traditional approaches to shape control use discrete transducers and lumped parameter modeling techniques. For real-time shape control these techniques can only address performance measures in a limited fashion, if at all.

Distributed parameter control, that is, the control of systems described by space and (usually) time, can more effectively address the spatial performance requirements dictated by the shape control problem. In addition to traditional temporal bandwidth requirements, shape control requires both a prescribed spatial bandwidth and a set of shapes that characterize the control task, for example, airfoil shapes for efficient flow control.

Distributed parameter system control techniques and spatially distributed transducers are well suited to the design and implementation of dynamic shape control in modern systems. In what follows modern robust multivariable control techniques are applied to the problem of dynamic airfoil morphing. Spatially distributed transducers and distributed parameter system design and analysis techniques are applied to seamlessly integrate multi-input/multi-output (MIMO) system design methodologies with dynamic shape control synthesis.

II. Airfoil Shapes and the Discrete Spectrum Parameterization

The machinery of modern control analysis and synthesis, although explicitly incorporating temporal frequency domain information for the synthesis of temporal servos, does nothing to address spatial performance and the synthesis of spatial servos. The distributed nature of the system to be controlled is either neglected

Received 21 December 2004; revision received 28 June 2005; accepted for publication 5 July 2005.

*Langley Distinguished Professor National Institute of Aerospace, Aerospace Engineering Department. Member AIAA.

or treated using ad hoc methods. Performance requirements for the shape control problem must be posed in spatial terms. Using MIMO techniques, one can construct an input/output relation representing a distributed parameter system (DPS) in a temporal and spatial frequency-domain. Given the success and availability of temporal frequency-domain tools in classical and robust, multivariable lumped parameter systems control theory, the introduction of spatial frequency transforms to distributed parameter systems and control follow naturally. An extensive treatment of spatial filtering concepts in distributed parameter control has been presented by Burke and Hubbard with applications to both active vibration control and dynamic shape control, including experimental validation.[7–9] Those techniques are applied here to the airfoil morphing control problem. The details of these techniques are beyond the scope of this paper; however, key results are highlighted herein where necessary.

Morphing from one shape to another requires that the morphing system use minimal energy during the process. Posing the control problem in terms of shapes that are easily and readily attainable by the system can achieve this goal. The control problem for achieving the desired airfoil shape can readily be posed in terms of controlling a set of orthogonal shapes. Any desired shape would then be represented by

$$y(x) = c_1\psi_1(x) + c_2\psi_2(x) + \cdots \tag{1}$$

where $\{\psi_i(x)\}$ are the orthogonal shape functions that represent the required component profiles and thus the shape control task.

The shape control problem is now parameterized and becomes a matter of deriving an input/output representation of the distributed plant in terms of the expansion (1).

III. Concept of EigenFoils

Many modern airfoils can be adequately described using the parameterization just described, that is, a limited set of orthogonal basis or eigenfunctions; for the sake of this discussion, we shall refer to these as *eigenfoils*. Consider for example the MH 20 pylon racer high-performance airfoil shown in Fig. 1.

The airfoil shape shown can be represented in decomposition on a basis of functions with a *discrete* spatial transform in a set of orthogonal functions, for example, a Fourier series. The upper portion of the airfoil shape for example can be decomposed as

$$y(x) = 0.0613\sin(\pi x) + 0.0203\sin(2\pi x) + 0.0048\sin(3\pi x) + 0.0054\sin(4\pi x) \tag{2}$$

which has a mean square fitting error of 0.0102 or roughly 1% and is shown graphically in Fig. 1, where Y is the airfoil thickness, X is the chordwise dimension, and C is the nominal chord length.

The discrete spectrum indicated by Eq. (2) and plotted in Fig. 1 indicates that to a reasonable approximation the airfoil shape has a finite discrete spatial bandwidth.

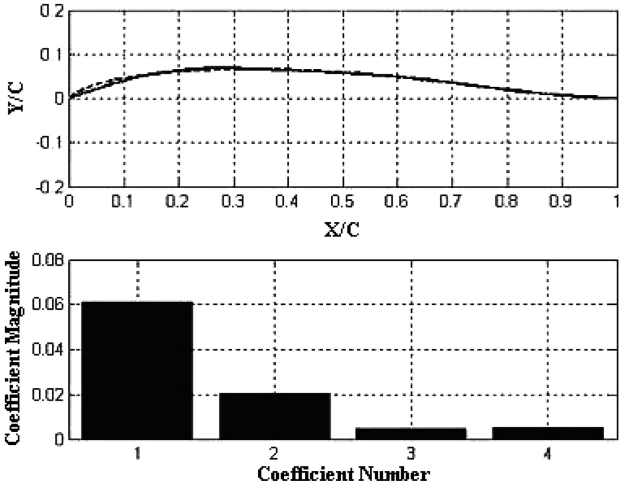

Fig. 1 Fourier-series approximation of the MH20 airfoil.

An interesting and somewhat intuitive interpretation of Eq. (2) is that the airfoil shape can be thought of as a supersposition of four distinct functions or basis shapes. Hence, if a control system is designed such that it can achieve each basis shape independently, then it can also synthesize the entire family of shapes represented by linear combinations of the basis. For the morphing airfoil problem, this family of shapes should by necessity span the performance envelope of interest.

Airfoils that can be adequately described using a limited set of orthogonal basis or eigenfunctions are therefore amenable and predisposed to achieving an entire family of shapes represented by linear combinations of those basis. This property can be used to guide the design of adaptive structures, which require morphing or dynamic shape control. Structural systems, which are themselves self-adjoint distributed parameter systems (e.g., Sturm–Louisville systems), readily admit orthogonal eigenfunctions and have preferred shapes governed by these bases. These so-called eigenfoils allow for seamless integration of dynamic shape control into the structural design of the overall system.

IV. Morphing Airfoil Design Considerations

In the remainder of this paper a proof-of-concept design is undertaken, and the application of the aforementioned techniques will be demonstrated by design and analysis. Consider the morphing airfoil system shown in Fig. 2.

The system consists of upper and lower flexible airfoil ribs joined together at their boundaries via pinned-pinned boundary conditions. Each rib or beam can be modeled as a Bernoulli–Euler beam with in-plane tension and structural damping. The displacement of each beam is therefore assumed to be expandable in a set of sinusoidal shape functions. For the pinned-pinned beam, these functions are orthogonal and therefore possess the property of spatial independence.

Our goal is to be able to command the shape of both the upper and lower airfoil ribs so as to assume the shape of the HF20 pylon racing airfoil shown in Fig. 1 and the family of shapes represented by any linear combination of its bases. The desired shape functions will be the first four sinusoids as given in Eq. (2). Table 1 and 2 are tables of the beam and actuator properties respectively used in the Plant model for the shape control task. We consider the shape control of only the upper rib modeled as a nondimensional pinned-pinned beam assuming that the lower rib could be controlled simultaneously in a similar manner.

For the purpose of control, we will use spatially distributed actuators in the form of NASA macrofiber-composite (MFC) actuators.[10] These actuators have good control authority, stability, and robustness properties and because they have spatial extent are well suited to the shape control task. The MFC has proven to be particularly useful in both rotary-wing and fixed-wing aeronautical applications. It has the desirable features of high-strain-energy density, directional actuation, conformability, and durability.[10]

Table 1 Airfoil rib material properties

Parameter	Value
Material	904 Stainless steel
Length	14.56 in. (369.8 mm)
Thickness	0.015 in. (0.381 mm)
Density	0.2815 lb/in.^{3} (7.8 gm/cm^3)
Modulus	3.047×10^7 psi (21.4×10^3 kgf/mm^2)

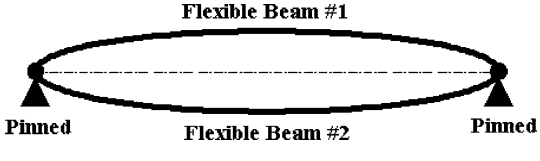

Fig. 2 Morphing airfoil configuration.

Table 2 Macrofiber-composite actuator material properties

Parameter	Value
Length	3.4 in. active segment (85 mm)
Width	1.1 in. (28 mm)
Thickness	0.01181 in. (.3 mm) (0.01281 film + bond)
Density	0.065 lb/in^3 (gms/cm^3)
Modulus	4.4×10^6 psi (30.336 GPa)
Static piezoelectric constant, d_{33}	8.267×10^{-9} in./V (4.6×10^2 pC/N)
Interstitial segments	0.12 in. (3 mm)

V. Actuator Placement and Input/Output Coupling

A considerable amount of work has been done in the characterizations of MFC actuation and the modeling of aerodynamic structures embedded with MFCs. Most notably, Cesnik et al. have developed accurate modeling techniques for beam, wings, and rotor blades with embedded anisotropic piezocomposite actuators.[11] These techniques are then used to spatially distribute MFC-type actuators in a wing or airfoil cross section in a progressive manner so as to maximize the induced stress for increased control authority. Additional tradeoffs are also possible between mass, structural integrity, power distribution, and the like.

Here we seek an actuator placement that will result in a balanced participation of actuation. To evaluate and decide on the proper actuator placement, we apply the technique of "harmonic balancing" described in Ref. 12 and repeated in condensed form here for clarity. In the shape control problem the goal is to drive the output of the distributed system (i.e., the upper airfoil rib) to each of the orthonormal shape functions $\{\psi_i(x)\}$ up to a discrete band limit $i = L$, both independently and in combination, that is,

$$y_{\text{desired}}(x, \omega) = \sum_{i=1}^{L} \beta_i(\omega)\psi_i(x) \tag{3}$$

The input coupling operators can be computed by considering the airfoil rib control problem as control of a nondimensional pinned-pinned beam. The desired shape functions are given in Eq. (2) as four sinusoids. The rib will be driven to the desired shape by abutting four MFC actuators, equally spaced over the length of the beam. As already discussed, four actuators are required in order to meet the bandwidth requirements of Eq. (2). Each actuator has the characteristics given in Table 2, a rectangular aperture, and is assumed for the sake of simplicity to have infinite temporal bandwidth.

VI. Morphing Airfoil Rib: Discrete Parameterization and the System Model

For control system design purposes the "Plant," which consists of the upper airfoil rib, is modeled as a Bernoulli–Euler beam with in-plane tension and internal structural damping. The model presented here follows closely the procedures outlined in Ref. 8. The governing equations for the airfoil rib including the control inputs from the four MFC spatially distributed actuators are

$$EI\frac{\partial^4 y(x,t)}{\partial x^4} - T\frac{\partial^2 y(x,t)}{\partial x^2} - \lambda\frac{\partial^3 y(x,t)}{\partial x^2 \partial t} + \rho A\frac{\partial^2 y(x,t)}{\partial^2 t} = m\sum_{i=1}^{4}\frac{\partial^2 V_i(x,t)}{\partial x^2} \qquad 0 < x < L \tag{4}$$

where EI is the rib/MFC composite structures flexural rigidity, λ is the structural damping coefficient, and ρ is the rib/MFC composite's mass per unit length.

The displacement of the airfoil rib is assumed to be expandable in a set of sinusoidal shape functions,

$$y(x,t) = \sum_{n=1}^{\infty}\sin\left(\frac{n\pi x}{L}\right)y_n(t) \tag{5}$$

with the Fourier coefficients being defined by

$$y_n(t) = \frac{2}{L}\int_0^L y(x,t)\sin\left(\frac{n\pi x}{L}\right)\mathrm{d}x \tag{6}$$

The input can be represented as a separable product of space and time for these so-called degenerate

$$V(x,t) = \sum_{i=1}^{4}\Lambda_i(x)u_i(t) \tag{7}$$

Assuming a uniform spatial distribution over the actuators aperture yields the result that

$$\Lambda_i(x) = h(x - c_i) - h[x - (c_i + \Delta_i)] \tag{8}$$

where c_i is the start of the aperture and Δ_i is its width. Similarly

$$\Lambda_i''(x) = \delta'(x - c_i) - \delta'[x - (c_i + \Delta_i)] \tag{9}$$

and if the control distribution is expanded in the requisite shape functions the right-hand side of Eq. (4) takes the form

$$\frac{\partial^2 V(x,t)}{\partial x^2} = \sum_{i=1}^{4}\sum_{n=1}^{\infty} q_{\text{in}}\sin\left(\frac{n\pi x}{L}\right)u_i(t) \tag{10}$$

The Fourier coefficients q_{in} of the MFC actuator distributions $\Lambda_i''(x)$ are described by

$$q_{\text{in}} = \frac{2}{L}\int_0^L \{\delta'(x - c_i) - \delta'[x - (c_i + \Delta_i)]\}\sin\left(\frac{n\pi x}{L}\right)\mathrm{d}x = -\frac{4n\pi}{L^2}\sin\left[\frac{n\pi}{2L}(2c_i + \Delta_i)\right]\sin\left(\frac{n\pi\Delta_i}{2L}\right) \tag{11}$$

The plant described in Eq. (4), through the discrete parameterization presented, can now be represented in traditional MIMO state-space canonical form.

VII. State-Space Canonical Form

Defining the time derivative of the nth Fourier coefficient yields

$$v_n(t) \equiv \dot{y}_n(t) \tag{12}$$

The nth shape of the governing equation can then be described as

$$\left[\frac{EI}{\rho A}\left(\frac{n\pi}{L}\right)^4 + \frac{T}{\rho A}\left(\frac{n\pi}{L}\right)^2\right]y_n + \frac{\lambda_n}{\rho A}\left(\frac{n\pi}{L}\right)^2 v_n + \dot{v}_n = \frac{m}{\rho A}\sum_{i=1}^{4} q_{\text{in}}u_i \tag{13}$$

In state-space form this becomes

$$\begin{bmatrix}\dot{y}_n \\ \dot{v}_n\end{bmatrix} = \begin{Bmatrix}0 & 1 \\ -\left[\frac{EI}{\rho A}\left(\frac{n\pi}{L}\right)^4 - \frac{T}{\rho A}\left(\frac{n\pi}{L}\right)^2\right] & -\frac{\lambda_n}{\rho A}\left(\frac{n\pi}{L}\right)^2\end{Bmatrix}\begin{bmatrix}y_n \\ v_n\end{bmatrix} + \frac{m}{\rho A}\begin{bmatrix}0 & 0 & 0 & 0 \\ q_{1n} & q_{2n} & q_{3n} & q_{4n}\end{bmatrix}\begin{bmatrix}u_1 \\ u_2 \\ u_3 \\ u_4\end{bmatrix} \tag{14}$$

where the state vector is defined as

$$\boldsymbol{X}_p \equiv [y_1 \quad v_1 \quad \cdots \quad y_4 \quad v_4]^T \tag{15}$$

and the control vector as

$$\boldsymbol{U}_p \equiv [u_1 \quad \cdots \quad u_4]^T \tag{16}$$

The first four output shapes are now the system outputs, and thus the output state vector can be defined as

$$\boldsymbol{y} \equiv [y_1 \quad \cdots \quad y_4]^T \tag{17}$$

Now the governing equation for the distributed parameter system consisting of the airfoil rib and MFC actuators can be written in state matrix form as

$$\dot{\boldsymbol{X}}_p = \boldsymbol{A}_p \boldsymbol{X}_p + \boldsymbol{B}_p \boldsymbol{U}_p \tag{18}$$

$$\boldsymbol{y} = \boldsymbol{C}_p \boldsymbol{X}_p \tag{19}$$

In this form we have achieved the parameterization that has the plant inputs as control voltages and the outputs are Fourier coefficients.

VIII. Morphing Airfoil Closed Loop Shape Controller Synthesis

A compensator for the morphing shape control task was designed using the loop-transfer-recovery (LTR) method of modern robust control. LTR is a structured method of compensator synthesis. Modern synthesis tools can be found in the robust control toolbox offered by MATLAB®. The design methodology is well known and well documented. The multivariable design is implemented using a linear-quadratic-Gaussian and a LTR design, which incorporates integral control and singular value matching at low and high frequencies. Because the shape expansion parameterization produces state-space models (for self-adjoint plants), other multivariable control design methods such as H_∞, μ synthesis, etc. could have been used.

A nominal plant as described by Eqs. (18) and (19) using the parameters of Tables 1 and 2 was constructed. A scaling of 10 • mils as outputs and $V/100$ as inputs was used for the compensator design and simulation. The airfoil rib was given a nominal tension of 4.9 lb. The modal parameters are given in Table 3.

The uncompensated forward-loop transfer matrix singular values for the nominal plant model are shown in Fig. 3. The plant has some directionality as seen. The reason for this directionality is reflected by the asymmetry in actuator coupling caused by the constrained interstitial spacing between actuators. Because the singular value plot is not highly directional, compensator design and implementation should be simplified.

Table 3 Beam/MFC dynamic parameters

Mode	Frequency, Hz	λ_n
1	34.576	0.00184
2	71.317	0.00191
3	112.18	0.00167
4	158.78	0.00456

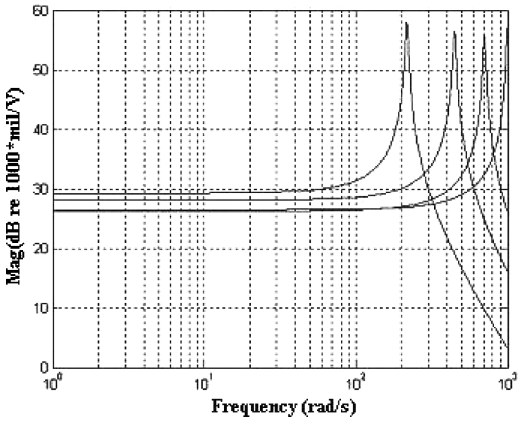

Fig. 3 Uncompensated nominal plant model singular-value-decomposition response.

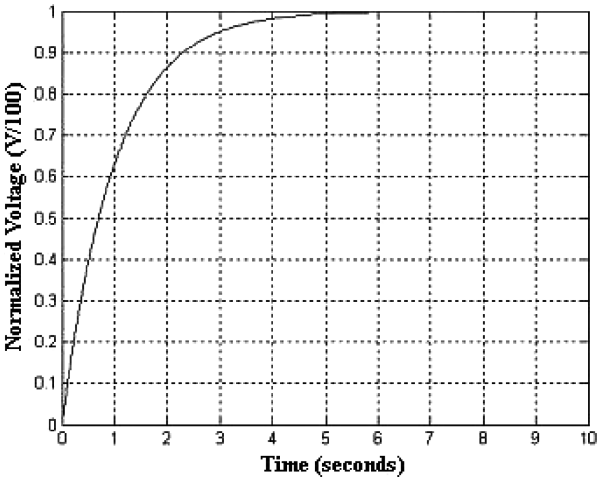

Fig. 4 Input command profile $U_0 = \text{Step}^*(1/s + 1)$.

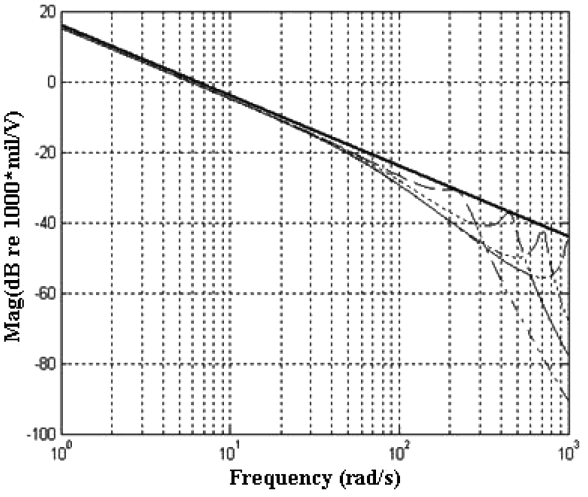

Fig. 5 Forward-loop singular value response for the target and recovered loop.

An input to the open-loop plant was formulated using the filtered step response profile shown in Fig. 4.

The design specifications for the control system design were as follows: 1) the nominal closed-loop system is stable, 2) the nominal closed-loop system exhibits zero steady-state error, and 3) the open-loop singular values are matched at ALL frequencies and lie above 20 db for all frequencies below 1 Hz. The design parameters for the compensator are listed here: μ, 0.025; ρ, 0.001; ω_c, 1 Hz; and order, 12.

The nominal plant of Fig. 3 was augmented with additional integrators in order to provide sufficient loop gain at low frequencies to satisfy the tracking requirement for all shapes. This augmentation also enhances disturbance rejection at low frequencies, for example, zero-steady-state error. Because the uncompensated plant has eight states and four inputs, the integrator-augmented design plant model has 12 states.

The target loop was constructed from the nominal plant. The singular values are plotted in Fig. 5 for the target and recovered loops. The parameter ρ is the so-called "cheap control" recovery parameter and can be used to adjust the bandwidth of the recovered loop. The smaller the parameter the better the recovery; small ρ implies large bandwidth and vice versa for large values of ρ. In practice ρ is adjusted to recover the target up to one decade above the crossover frequency of 1 Hz.

The forward-loop frequency response of Fig. 5 is nondirectional up to the recovered bandwidth limit. This will lead to a more decoupled shape control response in the closed-loop system as well as a more balanced participation of the MFC actuators.

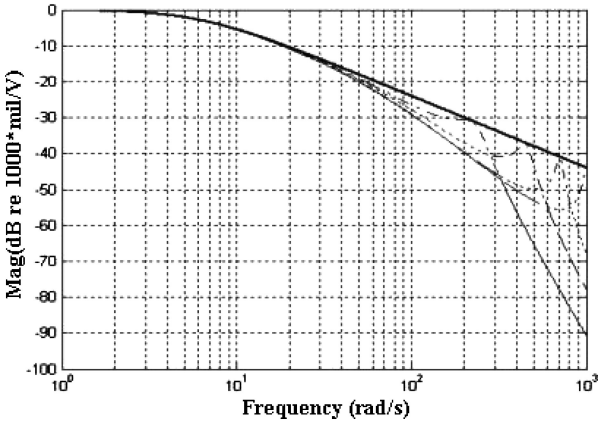

Fig. 6 Closed-loop singular-value response for the target and recovered loop: mu = 0.025.

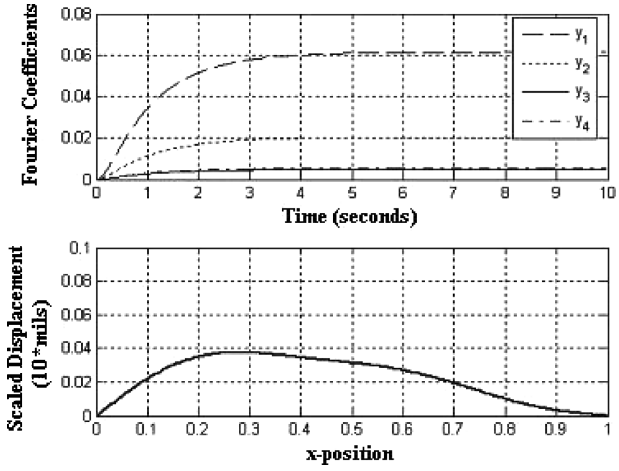

Fig. 7 Basis shape superposition for HF20 airfoil: HF 20 Pylon Racer Airfoil: $[0.0613, 0.0203, 0.0048, 0.0054]^T$ closed-loop response.

The closed-loop singular-value response for the target and recovered loop is shown in Fig. 6. The parameter μ sets the measurement noise intensity used to adjust the Kalman filter in the control synthesis process.

IX. Morphing Airfoil Closed Loop Shape Control Simulation

The compensator design of Fig. 6 was tested by observing the sequenced step response of each of the four basis sinusoid shapes as expressed in Eq. (5). Each shape was commanded individually by inputting a step input of 100 V as individual Fourier coefficients.

Because the controller decouples the basis shapes, its output can consist of any linear combination of the basis set of shapes. Recalling the airfoil decomposition illustrated in Fig. 1, the input to the controller is made to correspond to the Fourier components of the decomposed HF20 upper airfoil section. The result is shown in Fig. 7 as the reproduction of the HF20 profile. The profile achieved is accurate to within 1% rms and serves to validate the parameterization. The applied voltages were small, and hence the concomitant amplitudes are too small for practical application to real airfoil systems.

The operating voltage range of the MFC actuator is listed as −500 to 1500 V. Any practical application would involve optimizing the rib structure subject to and constrained by the aerodynamic loadings and MFC control authority.

X. Summary

A dynamic shape control proof-of-concept control system design and simulation has been applied to the problem of airfoil morphing. Effective airfoil morphing can result in significant increases in range and endurance in modern unmanned aerial vehicles. The loop-transfer-recovery method was used to construct a model-based compensator for closed-loop shape control. The design exploits the fact that the shape control task can be adequately and effectively parameterized by a band-limited set of orthogonal basis shapes. The control was applied to an airfoil model consisting of two beams that are pinned at the ends. The set of basis shapes chosen for the shape parameterization was sinusoids. The simulation involved commanding the upper beam to assume the profile of an HF20 high-performance airfoil. The commanded beam shape was achieved to within 1% error of the reference.

In any practical application of the techniques presented here, the airfoil should be morphed from a baseline reference shape, and the airfoil rib structure must be optimized to yield the required displacements given the aerodynamic loads and actuator control authority. Although the macrofiber-composite actuators might lack the control authority to achieve this in large-scale systems, there are a number of actuator options that when properly configured can be used to meet the desired objectives. This study therefore concludes that space/time parameterization, when coupled with representations of modern airfoil surfaces by a set of fundamental basis shapes, can achieve efficient aircraft structure morphing.

Acknowledgments

The author wishes to thank the NASA Langley Research Center for the support received to enable this study. The author would also like to thank the following individuals for their continued support: W. L. Fourney, A. W. Hubbard , K. V. Logan, A. A. Rodriguez, and A. W. Wilhite.

References

[1]McGowen, A. R., Horton, L. G., Harrison, J. S., and Raney, D. L., "Research Activities Within NASA's Morphing Program," Paper RTO-MP-36, NATO-RTO, Oct. 1999.

[2]Wlezien, R. W., Horner, G. C., McGowen, A. R., Padula, S. L., Scott, M. A., Silcox, R. J., and Simpson, J. O., "The Aircraft Morphing Program," AIAA Paper 98-1927, April 1998.

[3]Roth, B., Peters, C., and Crossley, W. A., "Aircraft Sizing with Morphing as an Independent Variable," AIAA Paper 2002-5840, Oct. 2002.

[4]Gano, S. E., and Renaud, J. E., "Optimized Unmanned Aerial Vehicle with Wing Morphing for Extended Range and Endurance," AIAA Paper 2002-5668, Sept. 2002.

[5]Spillman, J. J., "The Use of Variable Camber to Reduce Drag, Weight and Cost of Transport Aircraft," *Aeronautical Journal*, Vol. 96, No. 951, 1992, pp. 1–9.

[6]Peny, B., Cole, S., and Miller, G., "Summary of an Active Flexible Wing Program," *Journal of Aircraft*, Vol. 32, No. 1, 1995, pp. 10–15.

[7]Burke, S., and Hubbard, J. E., Jr., "Spatial Filtering Concepts in Distributed Parameter Control Systems," *Journal of Dynamic, Systems, Measurement, and Control*, Vol. 112, No. 4, 1990, pp. 565–573.

[8]Burke, S., and Hubbard, J. E., Jr., "Closed-Loop Dynamic Shape Control of a Flexible Beam," *Advances in Optical Systems*, edited by J. A. Breakwell, V. L. Genberg, and G. C. Krumwell, Vol. 1303, International Society for Optical Engineering, Bellingham, WA, 1990, pp. 321–323.

[9]Burke, S., and Hubbard, J. E., Jr., "Shape Control of Distributed Parameter Systems: Modeling and Performance Analysis," *Proceedings of 1990 American Control Conference*, Vol. 2, IEEE Publications, Piscataway, NJ, 1990, pp. 1552–1557.

[10]Wilkie, W. K., Bryant, G. R., High, J. W., Fox, R. L., Hellbaum, R. F., Jalink, A., Jr., Little, B. D., and Mirick, P. H., "Low-Cost Piezocomposite Actuator for Structural Control Applications," *Proceedings of the 7th Annual International Symposium on Smart Structures and Materials*, edited by Jack H. Jacobs, Vol. 3991, International Society for Optical Engineers, Bellingham, WA, 2000, pp. 323, 324.

[11]Cesnik, C. E. S., Ryan, S. P., and Palacios, R., "Effective Cross-Section Distribution of Anisotropic Piezocomposite Actuators for Wing Twist," *Smart Structures and Materials 2003: Smart Structures and Integrated Systems, Proceedings of SPIE*, edited by A. Baz, Vol. 5056, International Society of Optical Engineering, Bellingham, WA, 2003.

[12]Minto, K. D., and Knack, T., "Input/Output Oriented Computational Algorithms for the Control of Large Flexible Structures," Paper No. N90-10118, NASA Workshop on Computational Aspects in the Control of Flexible Systems, July 1988.